Sea Surface Temperature Variability in the Subtropical North-East Atlantic

I. Bashmachnikov[a,b]* , V. Lafon[a], A. Martins[a]

[a]IMAR-DOP/UAc, Cais de Santa Cruz, 9901-862, Horta, Azores, Portugal – (igorb, vlafon, anamartins)@notes.horta.uac.pt
[b]Dept. of Oceanography, St. Petersburg State University, 10th line 33/35, 199178, St. Petersburg, Russia

Abstract – AVHR images recorded during 2001-2004 were used to analyse Sea Surface Temperature (SST) spatial variability in the Subtropical North-East Atlantic. The individual images were decimated into 4.4 km and merged into 15-day averages. To reduce remnant non-physical noise, several filters were developed. Diurnal thermocline formation stipulated that during year round day-time SST images are warmer than night-times ones. SST stationary anomalies were obtained using a method of least-square fit of the all-region-average seasonal curve to the temperature variability at each pixel. The anomaly field reflects that the Mid-Atlantic Ridge (MAR) forms an efficient barrier for heat exchange between the western and eastern Atlantic basins. The MAR was characterised by colder SST values, possibly related to flow interaction with bottom topography. On the winter-time SST stationary anomaly field the Azores current could be distinguished.

Keywords: SST anomalies, the Mid-Atlantic Ridge, the Azores current.

1 INTRODUCTION

This work is devoted to investigation of the mean satellite derived SST fields in the Subtropical North-East Atlantic and their relation to the water dynamics in the region. The Subtropical Eastern North Atlantic (30-40^{o}N and 8-42^{o}E) is a region of complex space-time patterns of water temperature variability. Mean spatial temperature variations observed in the region are related to the influence of different branches of the Gulf Stream (Reverdin et al. 2003) such as, the Azores current (AzC, 34^{o}N) and the southern branch of the North Atlantic current (NAC, 45^{o}N), as well as, upwellings at the coasts of Portugal and Africa. Temporal variability is primary bound to the seasonal cycle. The high SST variability and considerable cloud cover are the reasons for non-physical noise to remain on the images after standard processing. Some additional filters were developed to reduce the noise.

2 METHOD

NOAA-12, -14, -16 and -17 AVHRR (1.1 km resolution) images, recorded at the Azores HAZO station from April 2001 to August 2004 were used. The images were processed using semi-automated imagery processes (TERASCAN), including the use of the MultiChannel Sea Surface Temperature algorithm (McClain et al. 1985) to compute Sea Surface Temperature (SST) values. It was previously proved that "erosion filters" (Gonzalez and Woods, 1992) was not very efficient to use in the region due to strong cloud cover and type. Therefore, we "widened" the recorded database including in the analysis all the pixels with no more than 6 (out of 8) contacts with clouds (Lafon et al. 2003). Afterwards, individual images were filtered by an SST band filter, which treated extremely low (<12^{o}C) and extremely high (>32^{o}C) SST values as errors (Lafon et al. 2003). Next, the individual images were binned into 4.4 km resolution by selecting in each 4*4 pixel box the highest SST value. This procedure also served as a filter to reduce remnant cloud contamination, typically resulting in too low SST values.

Due to cloud shading, individual images did not contain sufficient information on the SST spatial structure over the region thus, the images were merged into 15-day averages. Lack of data (i.e. mean pixel SST values computed mainly at the beginning or end of the averaging period), combined with strong seasonal trends, can produce false negative/positive SST anomalies. To avoid this, a 4-step method was developed. First, we eliminated mesoscale SST variability by spatially averaging daily SST images over the whole region. Second, maximum-likelihood linear trends (Huber 1981) for consequent 15-day intervals were calculated for each box, to evaluate the mean SST change over the period of interest. Third, the average temperature (T_{av}) for the 15-day SST trends was calculated. Assuming that the AVHRR-derived SST values had a maximum error (dT) of 0.5^{o}C (Walton et al. 1998), $T_1=T_{av}-dT$ and $T_2=T_{av}+dT$ values were computed as acceptable limits for the SST variability within the period of interest. Corresponding abscises of the T_1 and T_2 on the 15-day linear trend graphs are the dates D_1 and D_2. The latter formed time limits for the 15-day period, inside which SST mean change could be considered negligible. Finally, at each pixel the average of the dates for all valid SST values was calculated for every consequent 15-day period. If this time average did not lie within the corresponding [D_1 D_2] date interval, the pixel was blanked.

Analysis of the 15-day average images, obtained by the method described above, showed that three types of errors still remained: a cloud contamination error (anomalously low SST); a sensor error (unrealistic linear structures with anomalously low/high SST); and non-blank water SST values on land (night-time images, efficiently removed these by imposing a computed land-mask). Most of the errors, especially the "sensor" one, occurred in a random way and could be reduced, for the sets of overlaying images falling into a [D_1, D_2] interval, by substituting the outlier sensitive averages with a more robust median (MED). This significantly improved the results for the pixels where, at least, 3 images were overlaid. Unfortunately, in average, more than 50% of the valid pixels contained 2 or less overlying SST values. To enhance this initial filtering a "STD/MED" filter was applied. The region was separated in four 17x5^o sub-regions, in each of which the all-area average median (MEDM) was computed. The sub-regions were chosen such as to obtain a good compromise between having sufficient spatial coverage (i.e. having reliable spatially average MED in the presence of clouds), and keeping maximum homogeneity to retain main

spatial variability patterns: warm south-west; colder south-east; colder north-west; and coldest north-east. If, in a pixel, the SST value differed from the area MEDM more than STDM times, it was excluded from the computations. The STDM (in average 1.5°C) was computed as 3 times the standard deviation in each pixel (STD) for a 15-day period, averaged over the sub-region. In the case when all the SST values in the pixel were significantly far from the MEDM (e.g. in a cold narrow upwelling region), the SST value closest to the MEDM was kept as the filter output. The STD and the reliability (REL- number of valid data used for forming the MED) in each pixel-point were computed for further analysis.

The time-filter described above did not blank any of the valid pixels, but obviously did not improve the situation when all of the SST values in a pixel contained errors, or when the final SST value was derived from only one valid pixel. Taking all valid pixels on a 15-day average as 100%, the latter situation occurred, in average, in 35-50% of the instances in autumn-winter and in 20% – in summer. To blank the erroneous data points additional filters, based on SST spatial variability, were developed.

To remove most of the obvious cloud/sensor errors still persisting over wide areas, a "STD/MED" filter was ran again in a sort of iterative process, gradually improving the MEDM. This time the SST value was rejected (blanked) if it was more then 1°C different from the region MEDM and the STD in the pixel was more than 1°C. For the pixels, derived from only 1 SST value (REL=1, STD=0), only the critical distance from the MEDM was tested. The latter step could blank some valid pixels in the narrow cold upwelling strips near the continent, and to avoid this, the 300 km regions, adjacent to the land, were excluded from the filtering. The filter removed in average 2.5% and a maximum of 10% of all image pixels.

The "SST-jump" filter searches for high SST differences (jumps) between any two adjacent pixels and is based on the assumption of smoothness of the SST fields. Based on analysis of some meridional and zonal SST profiles we set the critical value of an SST jump to be 1°C. When a critical jump was found, the SST value, which was further away from a computed 120-point meridional or zonal linear trend (Huber, 1981), was blanked. To serve a base for further comparison the blanked pixel was temporary set to the linear trend value, thus allowing penetrating inside an anomalous region. The filter eliminated most of the cloud/sensor patches and strips, though also removed some valid pixels inside sharp upwelling fronts. It removed in average 2% and a maximum of 6% of all image pixels.

The "pixel-at-a-cloud" filter was designed to search for anomalous low SST values found inside or adjacent to cloud-covered regions. For the four 17x5° regions, spatially mean MEDM and STDM were re-computed. If the pixel SST value was significantly lower than the MEDM and more than 40% of the area around the pixel was covered with clouds, the pixel was blanked. The critical distance from the MEDM was set up to be 5 times the region STDM. This filter removed in average 0.1% and a maximum of 2% of all image pixels.

All of the previous filters failed when a contaminated region covered an area comparable to 25% of the region, or when a low SST region was surrounded by large cloud areas. In this case a "wild edit" filter was used to blank the SST values below a certain threshold in a defined sub-region. With this filter we removed in average 0.2%, and a maximum of 10% of the valid pixels.

These filters sequence removed in average 5% and in maximum 14% of the image pixels. At the end, an average of 60 to 80% of all the pixels on the 15-day averages were considered valid. The best spatial coverage was observed in summer. The resulting SST averaged images were smoothed with a 2D Savitzky-Golay second order filter with 16-point window. An interpolation under "small clouds", which had spatial dimensions 4 times less than the filter window size, did not change the SST structure, but permitted to get rid of a great deal of small-scale noise, improving the images visual interpretability. The interpolation "returned" in average 9% and up to 19% of all image pixels.

3 DAY- AND NIGHT-TIME IMAGES

The procedure was done separately for day- and night-time images. Day-time images contained a number of warm water patches not seen at night, probably related to diurnal thermocline formation under calm weather conditions. Night-time images were more cloud contaminated. The filters, described in the previous section, efficiently removed both types of errors. Comparison, pixel by pixel, of day and night images for the region showed that during oceanographic spring-summer (April-September) the day-time images were about 0.4-0.5°C warmer than the night-time ones, and during oceanographic autumn and winter (October-March) – only 0.2-0.3°C warmer. In summer, maximum of day/night differences, averaged over the image, was 0.9°C, but the difference in an individual pixel could reach several degrees. The mean day/night SST variability observed is consistent with the diurnal thermocline warming model (Gentemann et al. 2003), which, for NCEP-NCAR mean winds and insolation in the region (NCEP-NCAR), gave the mean day/night SST difference to be 0.4°C in spring-summer and 0.2°C in autumn-winter, respectively. Maximum day/night SST difference in the model (e.g. between 3am and 3pm) was 0.7°C for summer and 0.4°C for winter. Thus, the diurnal thermocline model can serve as a basis for day/night image merging.

4 SST STATIONARY ANOMALIES

To obtain mean SST spatial distribution over the period of observations, the SST stationary anomaly field was computed, using a method of least-square fit. At each pixel the all-region averaged seasonal curve was fitted to 15-day mean SST values at the pixel. The zero-order coefficient of the fit in a pixel-point was considered to represent a stationary SST anomaly in the pixel (Fig. 1). The method works as a time average, but it is much less sensitive for missing (cloud-covered) data points, and can be used for removing all-region mean time variability even for rather small periods of observations.

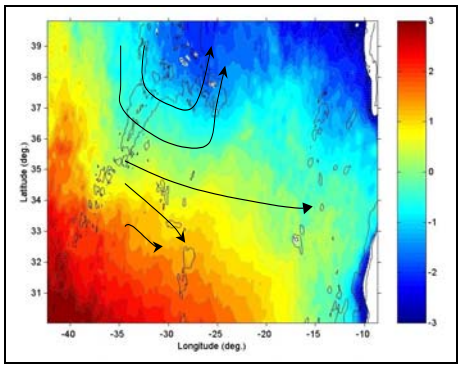

Figure 1. SST stationary anomaly field (^{o}C) for 2001-2004. Thin black lines represent 2000 m depth contour. Portugal and African coasts are seen on the east, and the Azores islands- at the top center. Thick black arrow-lines are yearly mean flow contours given by Stramma and Siedler (1988).

The stationary anomaly field (Fig. 1) showed the SST to decrease sharply (by 2-3^{o}C), at the western side of the Mid-Atlantic Ridge (MAR). Thus, warm water advected from the west is stopped by the MAR (Brower et al. 2000), which seems to form an efficient barrier to heat exchange between the western and eastern North Atlantic basins. The highest gradients were observed in the northern part of the region (Fig. 2), where the MAR rises from 4000 to 1000-2000m depth.

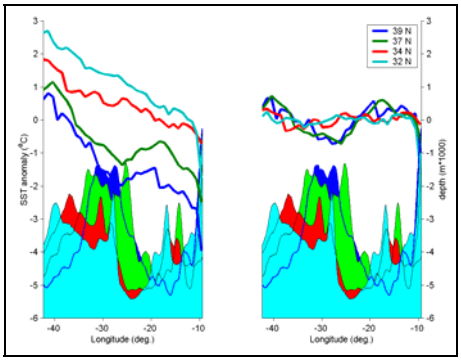

Figure 2. Left- stationary SST anomaly profiles at 32, 34, 37 and 39 ^{o}N. Right- detrended stationary SST anomaly profiles. Depth profiles (in 1000 m) are shown below the SST profiles.

Removing the general linear trend largely removed the effect of the warm water advection from the west (Fig. 2, right) and enhanced the effect of bottom topography on SST. Detrended SST longitude profiles (not including upwelling regions) showed significant (0.7-0.8) positive correlation between SST and water depth, e.g. SST was generally colder over the MAR. The correlation sharply decreased at 34-32^{o}N (at the AzC and just south of it), and increased again to the south. Some correlation between SST difference over and outside the MAR and the height of the MAR was found. The MAR cooling effect on SST was greater for shallower MAR.

Cooler SST over the MAR can be explained by topographic steering of an eastward moving barotropic flow. Equation for conservation of potential vorticity (Pedlosky, 1987) demands that a geostrophic flow to cross the ridge should first turn south, since it is allowed to move upslope only when reduces its absolute vorticity. The surface flow bowing south over the MAR between 37 and 41^{o}N (Fig. 1) was derived from *in situ* data (Stramma and Siedler, 1988). Other observations proved the MAR related water dynamics to be more complicated. Thus, at 47-55^{o}N an opposite northward bow of the currents was observed, accompanied by a southward turn at the eastern side of the MAR (Arhan, 1990; Pollard et al. 1996). In this case the flow did not go south to cross the depth contours, but seemed to retain its geostrophic balance, being topographically trapped at the 3000-4000m isobaths, then spreading north along the MAR until it found 3000-4000m deep Faraday and Charlie-Gibbs fracture zones to cross the ridge. At the same time, closer look at Fig. 1 reveal the eastern side of the MAR to be colder then the western one, which does not comply with the mechanisms described above. This is especially well seen at the north of the region, but less pronounced in the AzC (34^{o}N) and to the south. Baroclinic and ageostrophic processes could also play an important role in the MAR cooling effect. In fact, deep flow convergence to the MAR crest and dominating upward vertical velocities (though not reaching sea surface) were observed in TOPOGULF experiment around 48^{o}N (Arhan et al. 1989). Interactions of barotropic tides with topography could be another reason for the observed MAR cooling effect. Being a steep bottom rise, the MAR is an area of enhanced tidal mixing due to linear and non-linear barotropic tide enhancement (Kowalik and Polyakov, 1999), as well as, generation of internal tides (Kolomaitseva and Cherkesov, 1996). The tidally induced mixing increases the upward transport of colder water, which leads to colder SST.

The stationary anomaly SST field also showed persistent upwellings at the coasts of Portugal and Africa. At the coast of Africa a cold SST anomaly of 3^{o}C was observed, while near Portugal it was only 2^{o}C. In spring and summer both upwellings were stronger than during winter. In winter Portugal upwelling strength decreased 3 times, whereas the North African ones – less than 2 times. Spring-summer upwelling enhancement could be attributed to seasonal enhancement of southerly winds near the coast of Portugal and North Africa in summer (Tomzak and Godfrey, 2001).

Computed SST horizontal gradients helped to visualise main surface temperature fronts (Fig. 3).

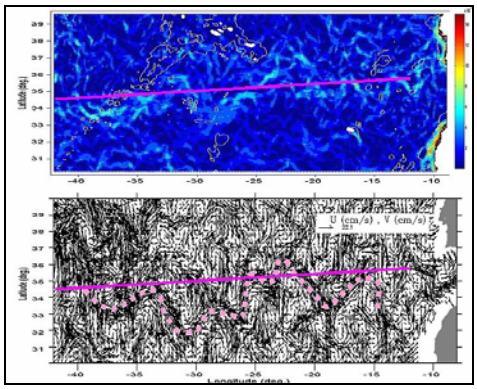

Figure 3. Above- SST stationary anomaly field gradients (^{o}C/km) in 2001-2004. White lines represent the 2000 m depth contour. Below- AVISO near-real time absolute geostrophic currents, February 2002 (adapted from Aviso). The thick dotted and strait lines represent the axis of the AzC obtained from altimetry data, and the mean position of the AzC obtained from the SST gradient field above, respectively.

The gradients were the strongest in the upwelling areas. The main regional Azores current, was hardly seen in summer, due to barring of internal water structure by seasonal thermocline (Gould, 1985). At the same time, in winter, it was clearly seen as an area of enhanced horizontal SST anomaly gradients (Fig. 3). Generally directed from west to east, it reaches the coast of Portugal, forming on its way series of quasi-stationary meanders.

5 ACKNOWLEDGEMENTS

This work was supported by the following: project ORPAM 2 (EC-Interreg IIIb-03/MAC/4.2/A2/ORPAM2), project DETRA (RAA–SRAPA/DRP–DETRA-2000-2003), funded by the Regional Directorate of Fisheries of the Azores, IMAR-DOP/UAc funds, and the Foundation for Science and Technology (Ministry of Science and Technology of Portugal) through two Post-Doctorate Fellowships. This support is greatly acknowledged. We would also like to acknowledge Margarida Rodrigues, Miguel Figueiredo, Ana Mendonca, Luis Macedo, Andre Couto, Neri Goulart, and Lara Coimbra from IMAR-DOP/UAc for initial imagery processing.

6 REFERENCES

6.1 References from Journals

Arhan, M., A. Colin de Verdiere and H. Mercier, "Direct observations of the mean circulation at 48^{o}N in the Atlantic ocean," Journal of Physical Oceanography, vol. 19, p.p. 161-181, 1989.

Arhan, M., "The North Atlantic Current and Subarctic Intermediate Water", Journal of Marine Research, vol. 48, p.p. 109-144, 1990.

Bower, A.S., H. Le Cann, T. Rossby, W. Zenk, J. Gould, Speer, K., P.L. Richardson, M.D. Prater, and H.-M. Zhang, "Directly measured mid-depth circulation in the North Atlantic Ocean,". Nature, vol. 419, p.p. 603-607, 2002.

Cipollini, P., D. Cromwell, M.S. Jones, G.D. Quartly, and P.G. Challenor, "Concurrent altimeter and infrared observations of Rossby wave propagation near 34° N in the Northeast Atlantic," Geophysical Research Letters, vol. 24, p.p. 889-892, 1997.

Gentemann, C.L., C.J. Donlon, A. Stuart-Menteth, and F.J. Wentz, "Diurnal signals in satellite sea surface temperature measurements," Geophysical Research Letters, vol. 30, No 3, p.p. 1140-1143, 2003

Gonzalez, R.C. and R.E. Woods, "Digital Image Processing", Massachusetts, Addison-Wesley Publishing Company, 1992.

Gould, W.J., "Physical oceanography of the Azores front," Progress in Oceanography, vol. 14, p.p. 167-190, 1985.

Huber, P.J., "Robust Statistics", New York, Wiley, 1981.

Kolomaitseva, E.M. and L.V. Cherkesov, "Generation of internal waves by an oblique barotropic tide, running against an underwater ridge," Isvestia AN, FAO, vol. 32, p.p.257-263, 1996.

Kovalik Z. and I. Polyakov, "Diurnal tides over Kashevarov Bank, Okhotsk sea," Journal of Geophysical Research, vol. 104, p.p. 5361-5380, 1999.

Lafon, V., A. Martins, I. Bashmachnikov, M. Melo-Rodrigues, and M. Figueiredo, "Sea surface temperature spatio-temporal variability in the Azores using a new technique to remove invalid pixels," Remote Sensing of Ocean and Sea Ice, Proceedings of SPIE, vol. 5233, p.p. 89-97, 2003.

McClain, E.P., W.G. Pichel, and C.C. Walton, "Comparative performance AVHRR-based multichannel sea surface temperatures," Journal of Geophysical Research, vol. 90, p.p. 11587-11601, 1985.

Pedlosky, J., "Geophysical fluid dynamics", New York, Springer, 1987.

Pollard, R.T., M.J. Griffiths, S.A. Cunningham, J.F. Read, F.F. Perez and A.F. Rios, "Vivaldi 1991- a study of the formation, circulation and ventilation of Eastern North Atlantic Central Water," Progress in Oceanography, vol. 37, p.p. 167-192, 1996.

Reverdin, G., P.P. Niiler, and H. Valdimarsson, "North Atlantic Ocean surface currents," Journal of Geophysical Research , vol. 108, p.p. 3002-3023, 2003.

Stramma, L., and G. Siedler, "Seasonal changes in the North Atlantic Subtropical Gyre," Journal of Geophysical Research , vol. 93, p.p. 8111-8118, 1988.

Walton, C.C., W.G. Pichel, J.F. Sapper, and D.A. May, "The development and operational application of nonlinear algorithms for the measurement of sea surface temperatures with the NOAA polar-orbitong environmental satellites," Journal of Geophysical Research, vol. 103, p.p. 27999-28012, 1998.

6.2 References from Websites

Aviso, Observing the Ocean from Space, http://www.aviso.oceanobs.com/

NOAA NCEP-NCAR: NCEP/NCAR Reanalysis Project. http://iridl.ldeo.columbia.edu/SOURCES/.NOAA/.NCEP-NCAR.

Tomczak, M., and J.S. Godfrey, 2001, "Regional Oceanography: An introduction," http://www.es.flinders.edu.au/~mattom/regoc/pdfversion.html